Physics – Uspekhi **52** (3) 209 – 224 (2009)

REVIEWS OF TOPICAL PROBLEMS

PACS numbers: **65.80.+n**, 73.23.Ad, 73.63.Fg

Transport properties of carbon nanotubes

A V Eletskii

DOI: 10.3367/UFNe.0179.200903a.0225

Contents

Abstract. The current status of experimental research on the transport characteristics of carbon nanotubes (CNTs) has been reviewed. Methods for measuring transport coefficients of CNTs have been considered. The available experimental data on the temperature dependence of thermal conductivity and electroconductivity of single-walled and multi-walled CNTs have been analyzed in terms of the ballistic mechanism of charge and heat transport.

1. Introduction

Carbon nanotubes (CNTs), due to their good electroconductivity and thermal conductivity and their high chemical, thermal, and mechanical stability, are considered one of the most promising subjects of nanoelectronics. They have already manifested themselves quite well as elements of such electronic systems as electron field emitters [1 – 4], supercapacitors [5], solar cells [6], nanoelectromechanical systems [7], and sensors [8]. Methods for producing CNTs have been considered in detail in reviews and monographs, as have their electronic, emission, sorption, and mechanical characteristics [1, 9 – 17].

In spite of the longstanding efforts of researchers from various laboratories in the world, the usage of CNTs in nanoelectronic devices has not yet spread commercially. This is due to several reasons. First, existing methods of CNT production do not yet allow synthesis of nanotubes with well defined geometry parameters such as diameter, length, chirality, and (for multi-walled CNTs) the number of layers. These parameters determine the electronic properties of CNTs. Thus a single-walled nanotube can possess either metallic or semiconductive properties, depending on the chirality indices. The forbidden gap width of such a semiconductive nanotube depends not only on the chirality but also on the diameter. The parameters of nanotubes synthesized by standard production methods [arc discharge, chemical vapor deposition (CVD), laser ablation (LA)] are usually characterized by a considerable spread. Large scale production of CNTs with predefined electronic characteristics presents a special technological problem. Second, the nanotubes produced through the use of standard methods usually contain a large number of structural defects that affect the electronic characteristics of the CNTs. Along with structural defects, there is some quantity of adsorbates, i.e., various molecules and radicals added to the external wall of a nanotube that change its electronic structure. Both the quantity of such violations of ideal CNT structure and their origin depend not only on its production method but also on the magnitudes of local parameters characterizing its growth. Among these parameters can be listed the temperature, velocity, and direction of gaseous flow, and the magnitude and the direction of the electrical field strength. One more reason for the rather slow introduction of nanotubes into applied fields relates to the very high cost of production of pure CNT samples. Samples of a material containing CNTs are usually highly contaminated with various admixtures such as carbon nanoparticles and metal catalyst nanoparticles enclosed in a multi-layer graphite envelope. Removal of these admixtures and purification of a sample up to level exceeding 90% present a very labor intensive technological problem involving repeatedly treating the sample with strong oxidizers, combined with centrifugation, filtration, and ultrasonication. This raises the price of pure CNT samples to a level exceeding $500 per gram, which precludes large scale application of this material.

Despite the above-mentioned difficulties, intense investigations have been performed in a large number of laboratories around the world that are addressed to establishing the physical and chemical properties of CNTs. Particularly considerable efforts are focused on investigating mechanisms of heat and charge transport and the relevant transport characteristics of nanotubes. These studies are of basic scientific interest because they offer the unique possibility to elaborate the transport characteristics of a 1D physical object. Such investigations are also important in terms of practice, since the magnitudes of the transport characteristics

A V Eletskii Russian Research Center 'Kurchatov Institute',
pl. Kurchatova 1, 123182 Moscow, Russian Federation
Tel./Fax (7-499) 196 99 78
E-mail: eletskii@imp.kiae.ru

Received 17 September 2008, revised 25 October 2008
Uspekhi Fizicheskikh Nauk **179** (3) 225 – 242 (2009)
DOI: 10.3367/UFNr.0179.200903a.0225
Translated by A V Eletskii; edited by E A Frimer

of CNTs determine the character of charge and heat transport in such systems and set the limitations for the maximum emission current in electron field emitters and other CNT-based nanoelectronic devices [18 – 20].

Due to the diversity of structural features of CNTs, which is due to a large variety of conditions of their synthesis, a considerable spread is inherent to the transport characteristics of nanotubes. Thus, the magnitude of the electrical resistance of CNTs reported by various authors ranges between 34 Ω and 10 MΩ. The measured magnitude of the thermal conductivity coefficient also ranges within several orders of magnitude. Such a considerable spread in measured values of transport coefficients is caused by both the uncontrollable defective structures inherent to CNTs produced by standard methods and the difficulties in experimental evaluation of these parameters. Moreover, single-walled CNTs (SWNTs) can possess either metallic or semiconductive properties, depending on their diameter and chirality. Therefore, their electroconductivity can range widely, especially at low temperatures. One should also mention the phenomenon of electron localization occurring in semiconductive CNTs at low temperatures that results in increasing dependences of the electroconductivity on the temperature and the electrical field strength. All these peculiarities complicate the transport problem, which doubtless hinders the calculation of emission characteristics of CNT-based field emission cathodes. This review contains an analysis of the current status of investigations into the transport characteristics of CNTs and consideration of the available experimental data in terms of known transport mechanisms.

2. Charge transport in CNTs

2.1 Single-walled nanotubes

The main contribution to the conductivity of CNTs is made by electrons. Therefore, the conductivity of CNTs is determined by the mechanism of electron mobility. In a defectless single-walled CNT at low temperatures, electrons pass through the nanotube without scattering, which corresponds to the *quantum ballistic* mechanism of conductivity. In this case, the resistance of a SWNT is expressed by the following equation [9 – 11]:

$$R = \frac{h}{4e^2} = \frac{G_0^{-1}}{2} = 6.47\ \mathrm{k\Omega}\,. \qquad (1)$$

Here, $G_0 = h/2e^2 = 7.72 \times 10^{-5}\ \Omega^{-1}$ is the quantum conductance of a quasi-1D conductor.

Equation (1) is generalized in a natural manner for nanotubes with defects whose length L exceeds the elastic scattering electron mean free path l_e [22]:

$$R = \frac{h}{4e^2}\,\frac{L + l_e}{l_e}\,. \qquad (2)$$

This equation corresponds to the *quasi-ballistic* mechanism of the conductivity of CNTs. In accordance with Eqn (2), the resistance of short ($L \ll l_e$) SWNTs does not depend on the temperature or the nanotube's length. Violation of this condition indicates a contribution by the *diffusion* mechanism to the charge transport. Due to the temperature dependence (usually increasing) of the number of scattering centers (acoustic phonons, structural defects, etc.), the elastic electron mean free path l_e decreases as the temperature rises. In accordance with Eqn (2) this is followed by the increasing temperature dependence of the resistance of SWNTs.

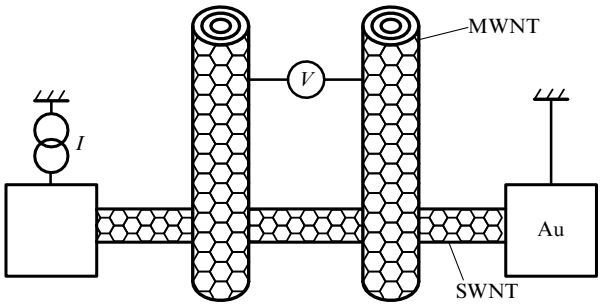

Figure 1. Schematic of the four-probe measurement of the dependence of the resistance of a single-walled nanotube on the length [22].

One should note that in treating the measurement data on the electroconductivity of CNTs, special attention has to be paid to the contribution of contacts to the resistance of a sample. Physical mechanisms determining this contribution have been analyzed in detail in the review article by Vorob'eva [21]. It should also be noted that the influence of contacts on the results of measurements can be practically excluded using the four-probe method of measurement, consisting of the determination of the resistance of a CNT vs the distance between the inner contacts.

Relations (1) and (2) have been justified by numerous experiments addressed to determination of the electroconductivity of highly purified SWNTs. As follows from these equations, the direct measurement of the resistance of an SWNT vs its length permits determining both its electronic characteristics and elastic mean free path l_e. Work [22] containing four-probe measurements of the resistance of an SWNT in the configuration shown on Fig. 1 presents a good example of such measurements. Note that the usage of the four-probe method permits excluding contact resistance from the measurement results, measuring the resistance of a CNT as a function of the distance between contacts. Multi-walled CNTs (MWNTs) were used as electrodes. SWNTs $\sim$ 1 nm in diameter grown by either the laser ablation method or chemical vapor deposition were selected from an array by means of an atomic force microscope (AFM). Then two MWNT electrodes were placed over the SWNT using an AFM manipulator. Cr/Au electrodes deposited by electron beam lithography were utilized as current leads. The conditions of the measurements and measured data are presented in Table 1.

Table 1. Resistance of various samples of SWNTs measured at room temperature for different distances L between the contacts; l_e is the elastic scattering electron mean free path evaluated on the basis of measured data and Eqn (2); L_{Au-Au} is the distance between the gold contacts [22].

No. of sample	R, kΩ	L, nm	l_e, nm	L_{Au-Au}, μm	Type of conductivity	Method of synthesis
1	1.5	95	408	2.7	Small gap semiconductor	CVD
2	37.0	100	17	5.6	Wide gap semiconductor	LA
3	2.7	150	358	1.0	Metal	CVD
4	6.3	140	143	0.6	Metal	LA
5	12.7	590	300	1.4	Metal	LA

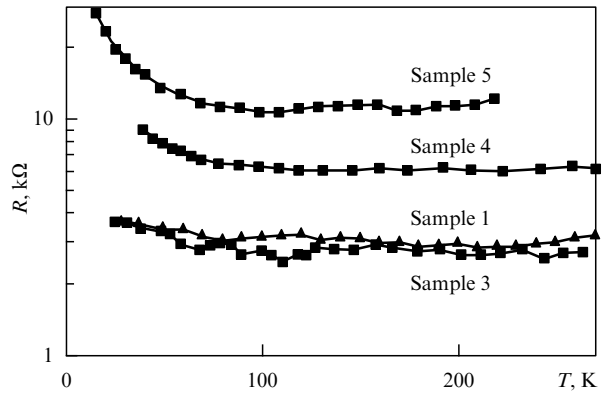

Figure 2. Temperature dependences of the resistance of some samples given in Table 1 [22].

As is seen from Table 1, a correlation between the length of a single-walled CNT and its resistance is barely observed. The resistance of two SWNT samples (1 and 3) exceeds notably that for quantum ballistic transport. The values of the resistance for samples 4 and 5 are in satisfactory agreement with (2), while sample 2 shows rather low conductivity compared to the others. Such a behavior can be explained by either bad contact or a high content of defects.

Figure 2 presents the temperature dependences of the resistance of some samples. As is seen, these dependences are very smooth, which is in accordance with Eqn (1). The low temperature increase in the resistance observed for samples 4 and 5 can be ascribed to the electron localization phenomenon, which is confirmed by the measured dependences of the resistance on the applied voltage.

The above-presented experimental data are in some contradiction with the measurement results [23], in accordance with which the resistance of SWNTs considerably exceeds the ballistic value (1) and depends on the temperature in a nonmonotonic manner. These results are shown in Fig. 3, presenting a comparison of the measured temperature dependences of a material containing SWNTs (a); several bundles connected in parallel (b); and an individual bundle with contacts spaced 500 nm apart (c). The measurements imply an increase in the resistance as the temperature rises from ~ 50 up to 580 K. Such a behavior can be explained by both enhancement of the intensity of the scattering of electrons on phonons whose content rises as the temperature increases and the corresponding increase in the defect content.

The results of the measurements [22, 23] given above are in a strong contradiction with earlier experimental data [24] that show a monotonically increasing temperature dependence of the resistance of an individual SWNT. In this experiment the electroconductivity of an SWNT was measured by both the two-probe and the four-probe method. The measurements were performed with both rectilinear and bent CNTs. Room temperature conductance of a rectilinear segment of the SWNT was measured at about $10^{-4}\ \Omega^{-1}$, which corresponds to a resistance of about 10 kΩ. This magnitude is in rough agreement with that of quantum ballistic conductance $2G_0 = 4e^2/h = 1.54 \times 10^{-4}\ \Omega^{-1}$. However, the conductance of a nanotube bent by 105° is about a hundred times lower and totals $\sim 10^{-6}\ \Omega^{-1}$. Figure 4 presents the temperature

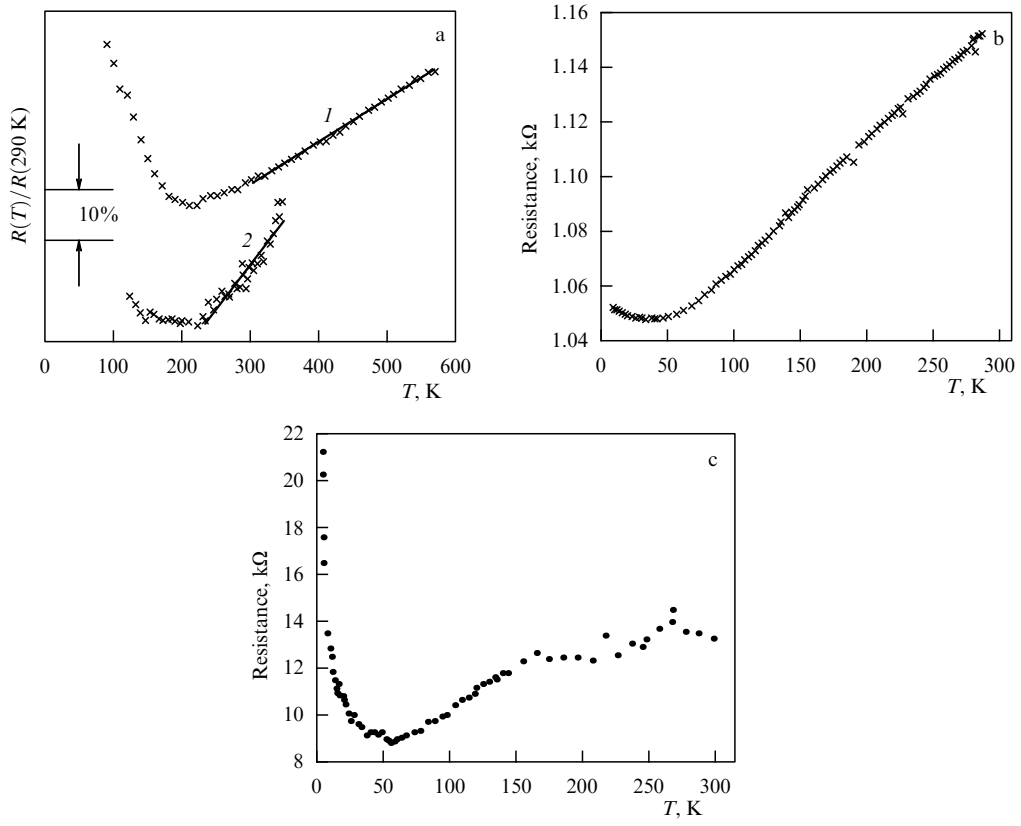

Figure 3. Temperature dependences of the resistance of SWNT samples [23]: (a) material containing SWNTs (curve *1* is the results of four-probe measurements; curve *2* is the results of measurements by the microwave absorption method); (b) two-probe measurements of several bundles connected in parallel; (c) four-probe measurements of an individual bundle.

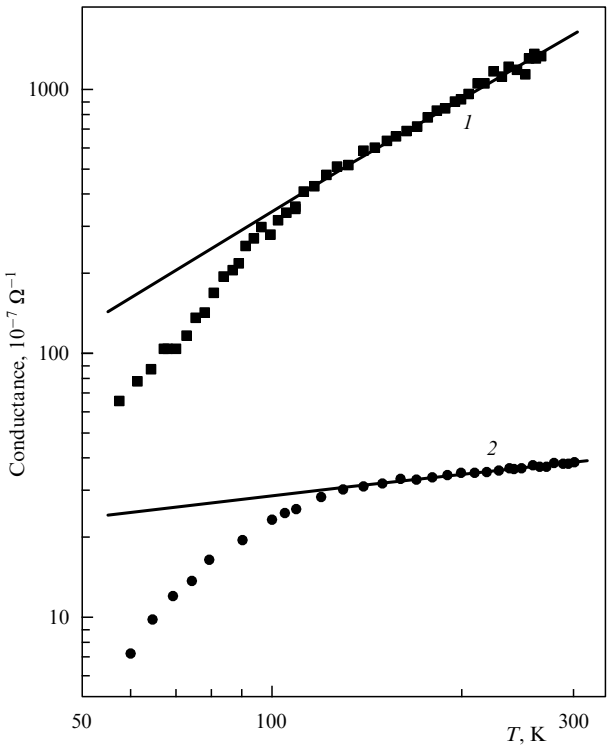

Figure 4. Temperature dependence of the electrical conductance of a bent segment of an SWNT measured by the four-probe (*1*) and two-probe (*2*) methods [24]. Solid lines represent the power-like approximation $G \sim T^{\alpha}$, where $\alpha = 1.4$ (*1*) and 0.26 (*2*).

dependences of the conductance of the bent segment measured by the two-probe and four-probe methods. One should note that the conductance of the contact is estimated as $\sim 8 \times 10^{-8}\ \Omega^{-1}$, which is much lower than that of the nanotube.

It should also be noted that the strong dependence of the conductance of SWNTs on the bending angle found in the above-described experiment [24] implies a possibility of using nanotubes as an active element of an electromechanical device transforming weak mechanical actions into an electrical signal (and back). Due to the miniature size and high sensitivity of nanotubes to mechanical action, such a transformer, the simplest example of which is a microphone, should possess good frequency characteristics.

An increasing temperature dependence of the conductance of individual nanotubes was observed also in the recent work [25]. Purified nanotubes synthesized by the HiPCO method (thermocatalytic decomposition of high pressure CO) were inserted into a 1% water solution of sodium dodecil sulfate (SDS), followed by ultrasonication and centrifugation. The suspension obtained was applied onto palladium electrodes which, using electron beam lithography, were placed on a highly doped silicon wafer covered with a silicon oxide layer 200 nm in thickness. The interelectrode distance was about 0.8 μm. An individual nanotube placed between the electrodes was selected by mean of an AFM. The current – voltage characteristics and gate characteristics of several nanotubes connected in parallel were measured by the two-probe method at various temperatures. Therewith a highly doped silicon wafer was used as a gate. The results of measurements obtained for metallic and semiconductive CNTs are shown in Figs 5 and 6, respectively. These data present power-like temperature dependences with the power

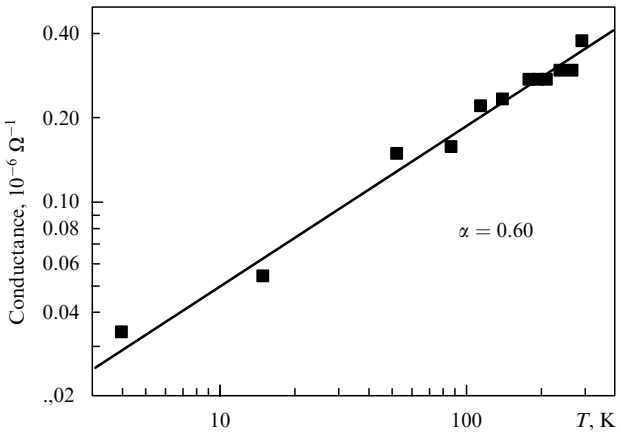

Figure 5. Temperature dependence of the electrical conductance of an individual metallic SWNT measured at a zero bias voltage. The dependence is well approximated by a power-like function with a power index $\alpha = 0.60$ [25].

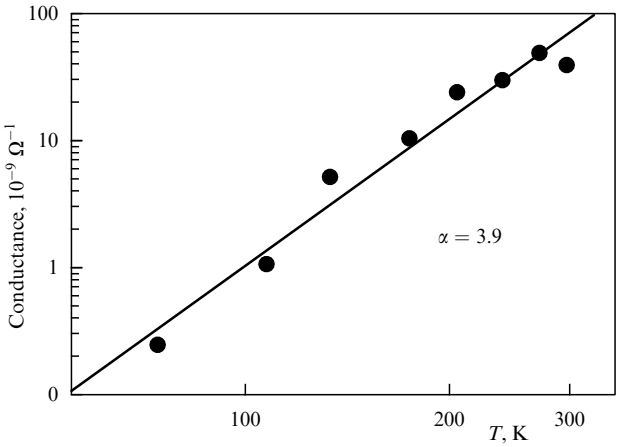

Figure 6. Temperature dependence of the electrical conductance of a semiconductive SWNT measured at a zero bias voltage. The dependence is well approximated by a power-like function with a power index $\alpha = 3.9$. The conductance at cryogenic temperatures is too low, which hinders its measurement [25].

index $\alpha = 0.60$ and 3.9, respectively. As is seen, the measured magnitude of the conductance G is much lower than the quantum limit G_0, which indicates a considerable contribution by the contacts to the total resistance of the circuit.

As follows from Eqn (2) the resistance of an individual nanotube can depend not only on the temperature but also on its length. This has been demonstrated by the results of recent studies [26, 27], where the conductance of individual SWNTs was also measured as a function of the applied voltage. The schematic of measurement is shown in the inset in Fig. 7. At low magnitudes of the bias voltage a defectless metallic CNT represents a conductor with quasi-ballistic conductivity, where the interaction of electrons with acoustic phonons is characterized by rather low intensity. At a high bias voltage (higher than 0.2 – 0.3 V), the intense scattering of electrons on optical phonons breaks their phase coherence, which causes a considerable contribution by the diffusion mechanism to electron transport, which is characterized by a linear dependence of the resistance on the nanotube's length. Long ($L > 1$ μm) nonsuspended SWNTs were placed on the surface of a silicon substrate covered by an oxide layer 500 nm thick

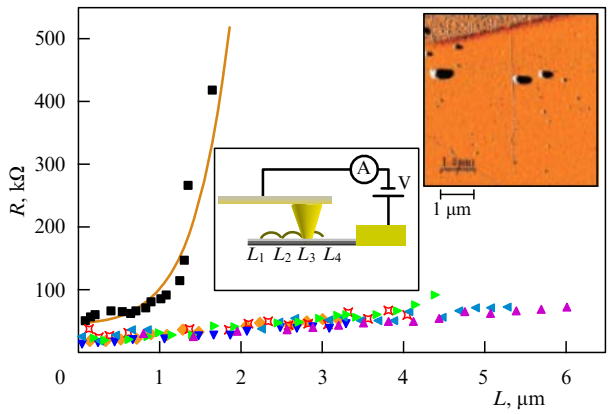

Figure 7. Low-voltage resistance vs length for CVD-grown SWNT (triangles and asterisks) and HiPCo SWNTs (squares) [26]. The experimental setup is shown schematically in the central inset. The upper inset presents the micro-image of a long nanotube partially gold-coated.

with the aim of exploring the dependences of the electroconductivity coefficient on the nanotube's length and the bias voltage. Nanotubes grown directly on the substrate were disordered and possessed quasi-ballistic conductivity.

In order to measure the dependence of the conductance on the length, a metallic SWNT was brought into contact with gold electrodes. In this case, the current – voltage characteristic was measured by using an AFM at a bias voltage varied within the range of ±2.2 V. A metal tip of the AFM was moved along the nanotube. The optimal contact was reached when the tip displaced the nanotube. The dependences of the differential resistance $R = \mathrm{d}V/\mathrm{d}I$ on the bias voltage and the interelectrode distance was determined by processing the current – voltage characteristics.

Figure 7 shows the low-voltage (bias voltage is about 0.1 V) dependences of the differential resistance on the interelectrode distance (L) measured for two types of SWNTs. Squares correspond to individual CNTs grown by the HiPCO method and subjected to ultrasonication in a surfactant with the aim of removing bundles. These nanotubes were then adsorbed on a silicon oxide substrate as a result of dispersion. Ultrasonication allows separation of a CNT from the bundles, while promoting the formation of structural defects. The rest of the data correspond to seven various metallic SWNTs grown directly on a substrate using the standard CVD method. A smoothly increasing interaction of the resistance with the length is a consequence of the interaction of electrons with acoustic phonons and structural defects. The relatively high content of defects inherent to the HiPCO SWNTs promotes the Andersen localization phenomenon. This phenomenon manifests itself in the exponential dependence of the resistance on the length found in the case of HiPCO nanotubes. Electrons moving along the nanotube undergo elastic scattering on defects conserving their phase. As is shown in Refs [28, 29], if the localization length L_0 is shorter than the electron mean free path relating to the elastic scattering on acoustic phonons, low-voltage charge transport is determined by defects and the resistance depends on the length in an exponential manner. This permits the determination of the magnitude $L_0 \sim 420$ nm for the HiPCO nanotube. On the other hand, the resistance of nanotubes grown by the CVD method depends linearly on their length, which corresponds to the Ohmic conductivity. One should note that the slope of this linear dependence that is determined by the low-voltage magnitude of the resistivity ρ_{low} amounts roughly to the same value for seven CNT samples ($\rho_{\mathrm{low}} \approx 10 \pm 2$ kΩ μm^{-1} at a contact resistance of about 18 ± 6 kΩ).[1] The resistance of a nanotube R is expressed through the mean free path of an electron relating to the elastic scattering on acoustic phonons l_{ac} by the following relation:

$$R = \frac{h}{4e^2}\,\frac{L + l_{\mathrm{ac}}}{l_{\mathrm{ac}}}\,.$$

This equation has been utilized for the treatment of experimental data obtained for SWNT grown by the CVD method, which resulted in the magnitude $l_{\mathrm{ac}} \approx 650 \pm 130$ nm.

At a high bias voltage ($V > 0.3$ V) electrons are able to excite optical phonons. In this case, the dependences of the differential conductance on the length measured along a nanotube 6 μm in length have a maximum near zero and then decrease at a short range inversely proportional to the length. As the bias voltage increases, the slope of these dependences and therefore the CNT resistance increases. Thus, at a voltage of 2 V, $\rho_{\mathrm{high}} = 320$ kΩ μm^{-1}. The average resistivity of seven CNTs grown by the CVD method measured at a voltage of 2 V is $\langle\rho_{\mathrm{high}}\rangle = 330 \pm 110$ kΩ μm^{-1}. The similar magnitude ρ_{high} was measured for HiPCO nanotubes. This means that the electron scattering on optical phonons prevails over the elastic scattering on lattice defects in the case of short nanotubes at a high bias voltage.

The above experimental data related to nanotubes shorter than 1 μm are in good agreement with the conclusion on the character of the charge transport in SWNT published earlier [27, 30]. However, if the interelectrode distance exceeds the indicated value, the dependence of the differential resistance $\mathrm{d}V/\mathrm{d}I$ on the length L shows a saturation which is changed by an abrupt decrease as the distance increases further.

The dependence of the resistance of a metallic individual SWNT on its length in low-voltage and high-voltage regimes was studied thoroughly in Ref. [27]. The distance between the contacts was varied within the range between 50 nm and 10 μm with the use of an AFM tip that was utilized as a movable electrode. The measurements indicate that at a low bias voltage the resistance of a CNT does not depend on its length for $L < 200$ nm. This implies that the ballistic mechanism of the charge transport occurs in short nanotubes. The measured dependence of the resistance on the length for longer nanotubes allowed determination of the low-voltage magnitude of the electron mean free path $l_{\mathrm{low}} \approx 1.6$ μm, which is in agreement with earlier measurements and calculations. At higher values of the bias voltage, the effect of current saturation has been observed for long nanotubes as the bias voltage increases. However, for short CNTs ($L < 500$ nm) the current is proportional to the bias voltage. The measurements performed at various L indicate that the high-voltage magnitude of the electron mean free path $l_{\mathrm{high}} \sim 10$ nm is about 100 times shorter than the relevant low-voltage value l_{low}. Calculations of low bias voltage

[1] One should differentiate between the resistivity of a CNT as any conductor that is expressed in the units Ω cm and specific resistivity accounting for the unit of the nanotube's length that is expressed by Ω cm^{-1}. These parameters are differentiated in the present article by the unit of measurement. This remark also relates to the thermal conductivity coefficient that will be considered in Section 3.

conductivity taking into account the electron scattering on acoustic phonons and high bias voltage conductivity taking into consideration the elastic scattering of electrons on optical phonons and the band boundary demonstrate good agreement with the experimental data [27].

Single-walled CNTs utilized in Ref. [27] were grown by the CVD method on a silicon substrate covered with a silicon oxide layer 200 nm in thickness. The catalyst was applied onto the substrate by means of lithography. Either an Au layer 50 nm in thickness covered with an adhesion Cr layer 5 nm thick or an Au layer 30 nm thick without an adhesion layer were used as contacts. The best contact was provided by gold electrodes without an adhesion layer. Cr/Au electrodes were subjected to annealing at a temperature of $\sim 600\,^{\circ}\mathrm{C}$ for improved contact between the metal electrode and the nanotube. All the measurements were performed with SWNTs possessing metal characteristics which were determined on the basis of measurements of the dependence of the conductance on the gate voltage. At a high bias voltage the magnitude of the saturation current for long nanotubes ranged within 19 – 25 μA. The transport characteristics of CNTs were measured by means of AFM under ambient conditions. The measurements were performed in a three-contact configuration (see Fig. 7) where the Au-coated tip of an AFM was used as the third contact. The bias voltage V_{sd} was applied to the source electrode while the AFM tip was used as a drain electrode. Therefore, the current was measured as a function of V_{sd} employing a current amplifier connected to the AFM tip. The second contact was applied by the lithography method and used for measuring the voltage drop V_{tt} between the tip and the drain electrode of the nanotube. This allowed determination of the voltage $V = V_{\mathrm{sd}} - V_{\mathrm{tt}}$ and therefore plotting the current – voltage characteristic corresponding to the left contact and the nanotube segment between this contact and the tip. The current – voltage characteristics for CNT segments of various lengths are measured by displacing the tip along the nanotube. Since the position of the left contact is fixed and the voltage drop related to the right AFM contact is subtracted, it is possible to compare the results of measurements obtained for CNT fragments of various lengths. The minimum fragment length that can be measured by this method depends on the stability of the AFM and the size of the tip and is estimated as $L \sim 50$ nm.

The dependences $I(V)$ measured for a metallic SWNT 10 μm in length at 6 various distances L allow discrimination between the low bias voltage region where the dependence has a linear shape and high bias voltage. Figure 8a presents the dependence of the low-voltage resistance of the CNT $R_{\mathrm{low}} = \mathrm{d}V/\mathrm{d}I$ on its length L. The magnitude R_{low} is practically constant within the range between 50 and 200 nm; however it increases as a result of the further increase in the length. The slope of this dependence presents the 1D resistivity $\rho = \mathrm{d}R_{\mathrm{low}}/\mathrm{d}L \approx 4\ \mathrm{k\Omega\ \mu m^{-1}}$. A similar value has been measured for some other samples of metallic SWNTs.

The 1D resistivity of a channel containing four subbands in a noncoherent limit is expressed though the following relation [9 – 11]:

$$\rho = \frac{h}{4e^2}\,\frac{1}{l_{\mathrm{e}}}\,, \tag{3}$$

where l_{e} is the elastic scattering electron mean free path. Measurements imply that the value of this parameter depends on the bias voltage. Treatment of the measured data obtained for low bias voltages results in $l_{\mathrm{low}} \approx 1.6$ μm. Since $L \ll l_{\mathrm{low}}$, ballistic charge transport occurs. In this case, the measured value of the resistance corresponds to that of the drain contact and is practically constant.

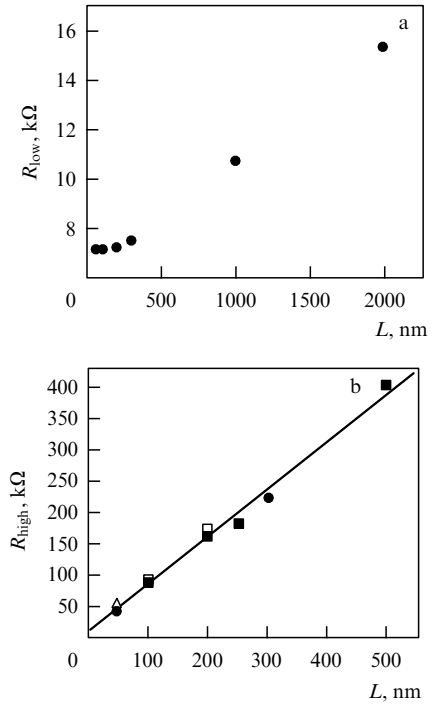

Figure 8. (a) Low-voltage differential resistance $R_{\mathrm{low}} = \mathrm{d}V/\mathrm{d}I$ vs L measured for an SWNTs 10 μm in total length and 1.8 nm in diameter. (b) High-voltage resistance $R_{\mathrm{high}} = \mathrm{d}V/\mathrm{d}I$ vs L measured for four various SWNTs 1.8 nm (●), 2 nm (■, □), and 2.5 nm (△) in diameter. The line presents the linear approximation of the measured data [27].

In the high bias voltage regime the slope of the current – voltage characteristic decreases as the voltage rises. In the case of a long channel the current saturates up to the level of about 20 μA. However, a different behavior has been observed for shorter channels ($L < 500$ nm). At a high bias voltage the current first rises proportionally to V; however, the slope of this dependence is lower than that in a low bias voltage regime. Figure 8b shows the dependence of the differential resistance $R_{\mathrm{high}} = \mathrm{d}V/\mathrm{d}I$ on L measured for CNTs of various diameters ($1.8 < d < 2.5$ nm). The slope of this dependence $\mathrm{d}R_{\mathrm{high}}/\mathrm{d}L = 800\ \mathrm{k\Omega\ \mu m^{-1}}$. As is seen, the high-voltage resistance is about 200 times as high as the relevant low-voltage magnitude. Processing this dependence in a high-voltage region by using (3) results in $l_{\mathrm{high}} \sim 10$ nm, where l_{high} is the high bias voltage magnitude of the electron mean free path relating to elastic scattering. Comparison of the values l_{low} and l_{high} indicates that the electron mean free path in a nanotube rises sharply as the bias voltage increases, which is caused by the electron localization phenomenon occurring at low bias voltages.

The above-described character of the dependence of the resistance of SWNTs on their length is inherent to even very long nanotubes up to a centimeter in size. This has been demonstrated in Ref. [31], where SWNTs up to 0.7 cm in length were studied. The nanotubes were grown on conducting doped Si wafers coated with an oxide layer 500 nm in thickness. Fe/Mo/aluminium oxide nanoparticles were utilized as a catalyst. Aluminium oxide nanoparticles were

dispersed in deionized water (250 ml), which was followed by insertion into the solution of 1.0 g $Fe(NO_3)_3$ and 0.24 g MoO_2-$(acac)_2$ (acac is acetylacetone). The suspension obtained was stirred for 24 h and subjected to ultrasound treatment for 1 h and then applied onto the Si wafer. A template was applied onto the Si wafers by means of a photoresist. The Si wafers were coated with thin films of Cr (50 nm)/Au (200 nm) by using the standard vacuum vaporization method, which was followed by the deposition of the nanoparticles mixture. This resulted in the formation of a triple catalytic layer of nanoparticles/Au/Cr. The nanotubes were grown in a homemade CVD furnace at a temperature of 900 °C as a result of circulation of the mixture of CH_4 (1000 sccm) and H_2 (200 sccm).[2] The above approach is characterized by simplicity because it does not require quick heating or the application of a high electrical field. One more distinctive feature of the approach applied is in the possibility of providing the electrical contact *in situ*.

Long nanotubes were studied by using a scanning electron microscope (SEM) operating at a low accelerating voltage (1 kV). Such a mode promotes an enhancement of the contrast of the image. Initially, metallic catalyst pads were charged negatively. Therewith the CNTs contacting the pads were also charged. Then the SEM was switched to the image magnification mode. The image of nanotubes contacting the catalyst pads was formed due to a difference between their potential and that of the substrate oxide layer. The geometry of the catalytic pad allowed the observation of the CNTs at low magnification. The distance between the neighboring catalyst pads was 4 mm. This method allows a considerable enhancement of the contrast of the image and permits one to obtain quickly the image of a CNT up to 1 cm in length. The duration of synthesis of CNTs up to 0.7 cm in length was 70 min. High magnification SEM images contained only one nanotube, while some images also contained several short CNTs oriented perpendicular to the long nanotube. Observations show that CNTs grow both in the direction of gas flow and also against the direction of gas flow (against the wind). The growth of a CNT stops upon the appearance of obstacles (such as a neighboring catalytic pad or the edge of the substrate) or as a result of cessation of the methane flow. Therefore, one can conclude that the fundamental limit of CNT growth has not yet been reached even for the centimeter size, and there is no evidence of such a limit.

The conductivity of an SWNT 4 mm in length was measured at about $2 \times 10^{-8}\ \Omega^{-1}$. A couple of nanotubes closing the gap are characterized by a decreasing current–voltage characteristic (using the substrate as a gate) with two different magnitudes of the threshold voltage. This indicates a semiconductive origin of CNT conductivity. AFM studies show that the diameter of nanotubes does not reach 5 nm, and the substrate is not contaminated with amorphous carbon even after completing the growth procedure.

Figure 9 compares the measured magnitudes of the resistance of SWNTs of various lengths. Processing these data obtained for long CNTs allows estimating the contact resistance at 15 kΩ. This means that the contribution of contacts to the resistance of long nanotubes ($R \sim 50$ MΩ) is practically negligible. The measured resistivity of long CNTs was about 6 kΩ μm^{-1}. Therefore, the resistance is proportional to the CNT length within four orders of magnitude.

[2] SCCM is cm^3 s^{-1} (at normal conditions).

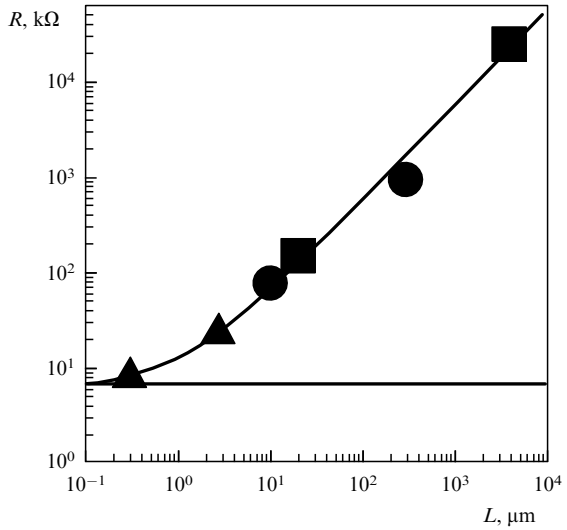

Figure 9. Resistance of SWNTs vs their length: ■ [31]; ● [32, 33], ▲ [34].

Processing the measured data obtained for another sample results in a resistivity of ~ 7 kΩ μm^{-1}, which corresponds to 1D resistivity of 1.4×10^{-8} Ω cm and comparable to the minimum resistivity measured to date for both metallic and semiconductive CNTs. Even a short fragment of a defective nanotube a centimeter in length would have much higher resistivity. This leads us to the paradox conclusion that the relative content of defects in CNTs a centimeter in length does not exceed that for the best CNT samples synthesized before now. In other words, the defect content barely depends on the nanotube's length and remains constant up to the centimeter size.

In summarizing the analysis of the data on the electroconductivity of SWNTs, one can conclude that nanotubes less than or of the order of 1 μm in length are usually characterized by room temperature resistance within 5–10 kΩ which corresponds to the ballistic conductivity mechanism. However, the conclusion on the ballistic character of the conductivity contradicts the results of measurements of the temperature dependence of the resistance, which is usually a monotonically increasing function of both the temperature and the nanotube's length. Violation of the ballistic character of conductivity is related to electron scattering on both acoustic phonons and structural defects. Therewith lowering of electron mobility as the temperature rises is caused by increasing the content of the acoustic phonons and structural defects. The characteristic magnitude of the elastic scattering electron mean free path estimated on the basis of experimental data amounts to about 1 μm, which can be considered the upper estimation of the length of SWNTs having ballistic conductivity.

2.2 Multi-walled nanotubes

The structure of MWNTs is usually not as perfect as in the case of SWNTs, therefore the ballistic mechanism of the conductivity is inherent to them to a lesser degree. However, an MWNT possesses a large number of conducting channels corresponding to the number of nanotube layers, which in turn enhances its conductivity. Since the diameter of an MWNT is considerably larger than that of an SWNT, electrical measurements with multi-walled CNTs are essentially simpler to perform and provide more reliable results.

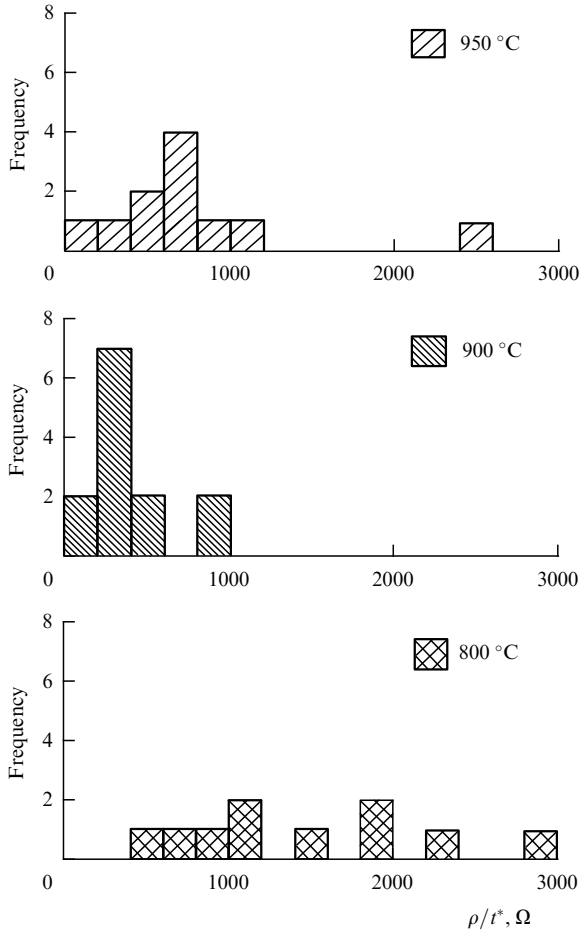

Figure 10. Histogram showing the distribution of nanotubes grown at temperatures of 800, 900, and 950 °C over the magnitude of the resistivity divided by the effective thickness of a nanotube t^* [35].

Measurements show that the conductivity of MWNTs depends notably on production conditions. This has been demonstrated particularly by the authors of Ref. [35] who compared the room temperature magnitudes of the conductivity of MWNTs grown at various temperatures (800, 900, and 950 °C) using the microwave plasma enhanced CVD method (PECVD). The results of the measurements presented in Fig. 10 indicate a correlation between the growth temperature of MWNTs and the resistance of individual nanotubes. The nanotubes grown at 900 °C possess the lowest resistance. Raman spectroscopy measurements show that these nanotubes have the best structure. The average magnitude of room temperature resistance of MWNTs amounts to 3.5 ± 2.6 kΩ.

The temperature dependence of the resistance of MWNTs is also characterized by a considerable spread even if these nanotubes are produced by the same setup. This is caused by the stochastic character of CNT growth, which results in a great variety of structural features of CNTs grown within the framework of the common procedure. The nanotubes grown in identical conditions can differ from each other in the number of layers, the type and the content of defects, length, and diameter. Such a diversity is reflected in the results of the measurement of the temperature dependence of MWNT conductance. This behavior can be seen from the measured temperature dependences of the electroconductivity of the six samples of SWNTs that are shown in Fig. 11 [36]. The

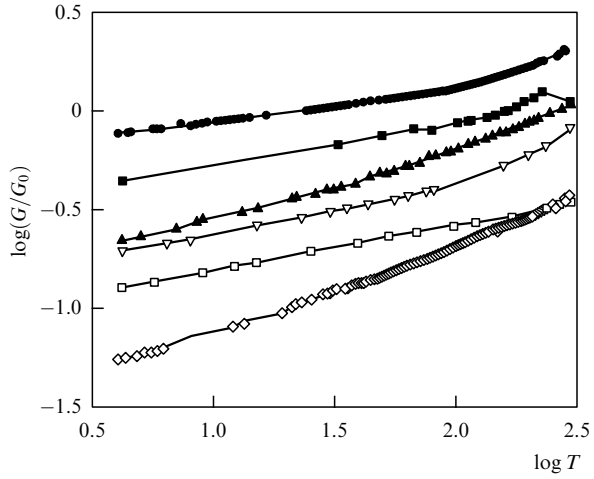

Figure 11. Temperature dependencies of the electrical conductance of various MWNT samples [36].

measurements were performed between 4 K and room temperature. The MWNTs were produced by the standard electrical arc method. The samples to be investigated were bundles containing from 3 to 6 individual CNTs. Some of the MWNTs in the bundles appeared to be damaged and seemingly only few or probably one of them contacted both metallic pads. As is seen from the data presented, the conductance of a CNT is of the order of the characteristic quantum value $G_0 = 2e^2/h = 7.7 \times 10^{-5}\ \Omega^{-1}$ and shows a monotonically increasing temperature dependence within the above temperature range. Such a shape of the temperature dependence of conductivity indicates a semiconductive origin of the charge transport in the MWNTs under investigation.

One can expect intuitively that the resistance of MWNTs is inversely proportional to the number of layers constituting the nanotube. This guess is supported by the results of measurements [37, 38] performed with nanotubes of a large cross section. For example, the authors of Ref. [37] studied MWNTs grown by the CVD method at 900 °C with the aid of Fe_2O_3 catalyst nanoparticles. An individual MWNT ~ 30 μm in length was selected in an arbitrary manner from a sample by means of a sharp tungsten tip. Then the nanotube was brought by means of a micromanipulator from the tip onto a transparent substrate. Further operations with the CNT were performed by means of a tungsten wire. Ti/Au electrodes were deposited onto the ends of the nanotube by the thermal evaporation technique. AFM measurements revealed that the titanium film was ≈ 10 nm in thickness, while the thickness of the gold film ranged within 50 – 100 nm. A similar procedure was applied to all the samples under investigation.

Successive shortening of the nanotubes was performed with the aid of a femtosecond laser ($\lambda = 800$ nm). The laser pulses had a duration of 90 fs, emission energy up to 1 mJ, and repetition frequency of 1 kHz. The sample moved relative to the laser beam by means of a computer-controlled 3D manipulator. The position of the laser beam relative to the nanotube could be changed to allow its shortening down to any length. To this aim, a ×100 microscope objective was used providing a focal spot size on the substrate on the level of 1 – 2 μm. It was found that the laser beam could occasionally displace the CNT from its initial position due to the occurrence of mechanical stress under the action of nonuniform heating. However, when taking precautions, a nanotube can stand 5 – 7 laser irradiation pulses without displacement.

To avoid thermal effects the current – voltage characteristic was measured at a low bias voltage ($|V| \sim 0.1$ V). Under this condition the dependence $I(V)$ had a linear shape. The total resistance of the sample was evaluated from the slope of the dependence $I(V)$ through the least squares method. This dependence was measured each time after shortening the CNT by using laser irradiation. The measures completed usually after about 5 shortenings. Then the sample was studied by means of a field emission scanning electron microscope (FESEM) in order to refine the parameters of the nanotube. The results of measurements are shown in Table 2. As is seen, the nanotube resistivity ρ_{CNT} ranges between 0.33 and 1.48 kΩ μm^{-1} (average magnitude is 0.69 kΩ μm^{-1}). The spread is probably caused by differences in the quantity and the structure of defects occurring in various CNTs. The measured value of the contact resistance ranges within 1.2 – 5.3 kΩ μm. As is seen, large diameter multi-walled nanotubes have rather low resistance, so that the charge transport in relevant devices is limited mainly by the contact resistance.

Obviously, all the layers constituting an MWNT contribute to its conductivity. However, exploration of the electrical characteristics of MWNTs meets with difficulties relating to the necessity of providing a reliable contact for all the layers of the CNT, otherwise the measured conductance would be notably lower than its true value. In this connection, one should consider Ref. [38] where special attention has been paid to ensuring a reliable contact for all the layers making up the MWNT. These measurements, demonstrating a record magnitude of MWNT conductance, are based a new method according to which the contacts are formed in the course of CNT synthesis. This provides high quality contacts for all the layers of the nanotube. The electrical properties of a large diameter MWNT are studied *in situ* by means of an SEM. The measured conductance exceeds considerably $2G_0$, which indicates the quasi-ballistic conductivity of the MWNT.

High aspect ratio individual nanotubes were grown by the PECVD method with a hot filament. A tungsten filament was utilized as a substrate and small intrusions of iron into the filament (at the level of 0.002 at.%) were used as a catalyst. The nanotubes were grown under the flow of methane (10 sccm) and hydrogen (50 sccm) at a total gas pressure of 25 Torr, discharge current of 50 mA, and voltage of $\sim$ 500 V. The substrate temperature was about 750 °C. The rectilinear nanotubes synthesized ranged between 6 and 30 μm in length and were arranged on the substrate with a surface density of not less than 10^6 cm^{-2}. Transmission electron microscope (TEM) observations have shown that the outer and internal diameters of the nanotubes were 100 and 50 nm, respectively. X-ray diffraction measurements did not indicate any notable structural damages or contaminations in the CNTs under investigation. Since the nanotubes were grown directly on the tungsten filament, their reliable electrical contact with the filament was ensured. As a second electrode a tungsten filament with a tip radius of 100 nm was also used. This filament was inserted into an SEM chamber and the tip moved there until contact with an individual nanotube was made.

Before measuring the current – voltage characteristics, a low voltage was applied between the movable probe and the nanotube, which promoted electrical discharge and local heating. This resulted in welding of the tungsten tip to the nanotube, forming a reliable electrical contact. As distinct from the standard two-probe or four-probe approaches to measuring the conductance of CNTs, when only external layers of the nanotube are in contact with current leads, in the present approach a reliable contact is provided for all the inner layers of the nanotube. One more advantage of the approach under consideration is that pure CNTs are grown directly on the conducting substrate, so that conductivity can be measured inside the SEM chamber without additional procedures such as purification, separation, or other operations which are utilized in standard methods and eventually can damage or contaminate the nanotubes.

The current – voltage characteristic of an individual MWNT is shown in Fig. 12 [38]. As is seen, this dependence has a linear shape within the range of the applied voltage, $\pm$0.2 V. One can conclude from this dependence that the MWNT under investigation possesses metallic properties and its resistance is 34.4 Ω. Metallic CNTs are very stable, while the energy of electrons (holes) is insufficient for the excitation of optical phonons. The excitation of optical phonons is possible if the applied voltage is out of the range ($\pm$0.2 V). In this case, the conductivity is determined by electron scattering on optical, but not acoustic, phonons, which results in the current saturation effect. The enhanced energy consumption due to electrical current passage promotes destruction of the ballistic conductivity mechanism. As is shown in Ref. [39], an MWNT breaks down at a dissipated power exceeding 300 μW. In the experiment under consideration [38], the total current of 7.27 mA is reached at a bias voltage of 0.25 V, which corresponds to a current density of 10^8 A cm^{-2} and dissipated power of 1.82 mW. Such an extraordinarily high value of dissipated power can be explained assuming the ballistic mechanism of charge transport in the MWNT under investigation. This assumption is confirmed by the results of measurements of the current – voltage characteristics of a shortened MWNT, which hardly differ from those for the initial CNT. This implies a ballistic character of conductivity of the MWNT. The measurements show that in this case the electron mean free path is as long as 25 μm, which exceeds by many times the estimations of other authors [40, 41].

As is seen from Fig. 12, the measured magnitude of the conductivity of MWNTs at a zero bias is about $460G_0$. This value exceeds considerably the results of other measurements

Table 2. The results of measurements of the resistance of MWNTs of various lengths [37].

Sample	Distance between contacts, μm	Diameter, nm	Resistivity of the CNT, kΩ μm^{-1}	Contact resistivity, kΩ μm	Contact resistivity, $\mu\Omega$ cm^2
1	10.0 ± 0.1	225 ± 10	1.48 ± 0.02	1.3 ± 0.2	4.6 ± 0.7
2	10.0 ± 0.1	210 ± 10	0.51 ± 0.02	1.2 ± 0.2	4.0 ± 0.7
3	10.0 ± 0.1	130 ± 10	0.79 ± 0.02	4.2 ± 0.4	8.6 ± 1.0
4	4.0 ± 0.1	83 ± 10	0.33 ± 0.04	4.4 ± 0.8	6.0 ± 1.2
4*	4.0 ± 0.1	83 ± 10	0.33 ± 0.01	5.3 ± 0.3	6.9 ± 0.9

* The data given in the two last rows relate to different types of contacts.

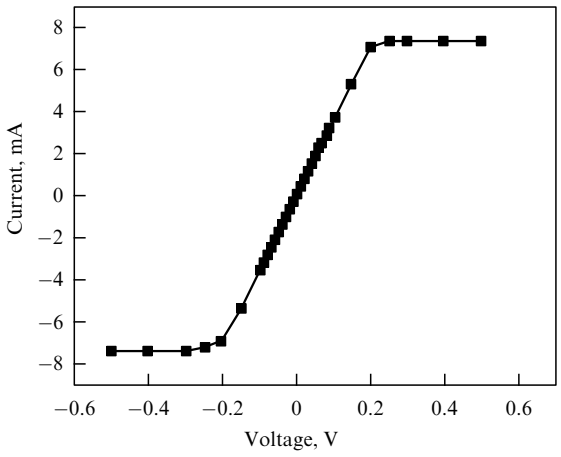

Figure 12. Current – voltage characteristic of an individual MWNT [38].

for individual nanotube, which usually total less than $2G_0$. The main distinguishing peculiarity of the experiment [38] consists in ensuring a reliable contact for all the nanotube walls, while in preceding experiments a reliable contact was provided for only in the outer layer of the CNT.

A multi-walled CNT with outer and inner diameters of 100 and 50 nm, respectively, and an interlayer distance of 0.34 nm contains no more than 74 layers. Even assuming that each layer possesses metallic properties and has a conductivity of $2G_0$, one can expect that the conductivity of such a nanotube does not exceed $148G_0$, which is notably less than the measured magnitude of $460G_0$. As is known, the forbidden gap width of a semiconductive CNT is inversely proportional to its diameter. Therefore, almost all the layers composing the MWNT under consideration have a negligible forbidden gap width (much less than the temperature) and can be considered metal conductors, whose conductance does not depend on such structural features as diameter and chirality. Nevertheless, the reason for such a high magnitude of conductivity of the MWNT still remains unclear.

Summing up this analysis of experimental data on the conductivity of multi-walled nanotubes, one should note that the magnitude of the conductance can exceed the value G_0, specific for the ballistic conductivity. This indicates the contribution of a large number of layers to the charge transport so that the partial contribution of each layer is of the order of G_0. However, the occurrence of a temperature dependence of the conductance excludes a purely ballistic mechanism of charge transport. Apparently, there exists a combination of ballistic and diffusion mechanisms of conductivity, so that the specific contribution of each of these is determined by both the synthesis parameters and the conditions of the measurements.

3. Heat transport in CNTs

The thermal conductivity of CNTs is determined by phonons, so that the role of conduction electrons is negligible [42, 43]. *Ballistic* heat transport occurs when phonons transfer energy without scattering, so that the characteristic phonon mean free path relating to the scattering on phonons and structural defects exceeds the length of the nanotube. The simplest description of ballistic phonon thermal conductivity corresponds to a high-temperature limit, which takes place at $\hbar\omega \ll T$ (ω is the characteristic phonon frequency, T is the temperature). In this case, the thermal conductance of each phonon channel is determined by the quantum magnitude $G_{\rm th}$, which has the form [43]

$$G_{\rm th} = \frac{\pi^2 k^2 T}{3h} = 9.46 \times 10^{-13} \left(\frac{\rm W}{\rm K^2}\right) T. \qquad (4)$$

The thermal conductance of a CNT is expressed as the product of the quantum conductance $G_{\rm th}$ and the total number of phonon channels $N_{\rm p}$ in the nanotube. The latter is a triple number of atoms in a unit cell $2N$, where N is expressed through the chirality indices (n, m) of the nanotube as [9 – 11]

$$N = \frac{2(n^2 + m^2 + nm)}{d_{\rm R}}\,. \qquad (5)$$

Here, $d_{\rm R}$ is the greatest common divisor of $(2n + m)$ and $(2m + n)$. For a CNT having the *armchair* structure and chirality indices (n, n), $d_{\rm R} = n$ and $N = 6n$. For example, a single-walled $(10, 10)$ CNT (diameter 1.4 nm) has $N_{\rm p} = 120$ phonon channels, while a $(200, 200)$ CNT (diameter 27.5 nm) has $N_{\rm p} = 2400$ phonon channels. Therefore, the ballistic thermal conductance of $(10, 10)$ and $(200, 200)$ CNTs amounts to $120G_{\rm th}$ and $2400G_{\rm th}$, respectively.

The scattering of phonons on structural defects and admixture centers can be taken into account in a manner that is similar to the above-considered description of the quasi-ballistic mechanism of electroconductivity of CNTs by introducing the correcting factor $k_{\rm d} = (L + l_{\rm p})/l_{\rm p}$. Here, $l_{\rm p}$ is the phonon mean free path relating to the elastic scattering and L is the nanotube's length. In accordance with this approach, the thermal conductance of a nanotube with a quasi-ballistic mechanism of heat conductivity is expressed by the relation

$$G = G_{\rm th}\, N_{\rm p}\, \frac{l_{\rm p}}{L + l_{\rm p}}\,, \qquad (6)$$

where the quantum thermal conductance $G_{\rm th}$ and the number of phonon channels $N_{\rm p}$ are given by the above relations (4) and (5). Such an approach to describing the heat conductivity of a CNT is quite convenient for the analysis of experimental data because it allows one to make a conclusion relating the specific mechanism of heat transport on the basis of the analysis of measured dependences of thermal conductance of a CNT on the temperature and its length.

As follows from Eqn (6), the thermal conductance of a long nanotube ($L \gg l_{\rm p}$) is inversely proportional to its length. Therefore, the thermal conductivity

$$\kappa = \frac{GL}{S} \qquad (7)$$

(S is the area of the cross section of the nanotube perpendicular to the direction of the heat flow) does not depend on its length L. This conclusion is similar to the Ohm law for the electroconductivity of conducting materials and is named the Fourier law for heat conductivity. The Fourier law is obviously violated in the case of the prevalence of the ballistic mechanism of heat transport, when the thermal conductance of a nanotube does not depend on its length. In this case, in accordance with Eqn (7) the thermal conductivity of a CNT is inversely proportional to the nanotube's length. However, detailed measurements of the dependence of the

thermal conductivity on the length of a nanotube performed recently [44] show that the Fourier law can be violated even on the condition that the nanotube's length L exceeds considerably the characteristic value of the phonon mean free path l_p. Multi-walled CNTs produced by the standard electrical arc method and ranging between 10 and 33 nm in diameter, as well as boron nitride nanotubes (BNNTs) up to 10 μm in length and 30–40 nm in diameter, were used in this experiment. An individual nanotube was placed by means of a piezomanipulator into a testing device that was inserted into the chamber of an SEM. The testing device contained suspended SiN_x plates and Pt film resistors that played the role of both heater and temperature sensor. The thermal conductance of the nanotube was determined on the basis of measurement of the temperature by means of the sensor at some specified power supply. The geometry of the sample was measured by the use of an SEM. The thermal conductance of samples was measured utilizing contacts fabricated from the platinum compound $(CH_3)_3(CH_3C_5H_4)Pt$ and having a rectangular shape. The thermal resistance as a function of the nanotube's length was evaluated performing sequential measurements of the thermal conductance at various positions of one of the contacts along the nanotube. These dependences deviate notably from a straight line, which indicates a violation of the Fourier law for the thermal conductivity of nanotubes. Thus, a sample of CNTs 5 μm in length having the room temperature thermal resistance of 5.87×10^7 K W^{-1} shows an increasing power-like dependence of the thermal resistance on the length with the power index of $\beta = 0.6$, while the Fourier law requires $\beta = 0$. The thermal resistance of a sample of BNNTs 5.33 μm in length is 7.71×10^7 K W^{-1}, while $\beta = 0.4$. Note that the contribution of the contact resistance to the total resistance of both samples does not exceed 25%. It is important to stress that the thermoconductance of nanotubes deviates from the Fourier law even when the phonon elastic scattering mean free path l_p is much shorter that the nanotube's length L. Thus, the magnitude l_p, estimated on the basis of the measured thermal conductance coefficient, is about 30–50 nm, which is considerably shorter than the nanotube's length.

The thermal conductivity of a cloth-like layer of an SWNT was measured in Ref. [45] within the temperature range between 8 and 350 K. The nanotubes were synthesized by the electrical arc method with the use of graphite electrodes filled with a Y and Ni powder catalyst. This approach permits the production of a cloth-like layer consisting of high purity tangled nanotube bundles. Each of the bundles contains from tens to hundreds of nanotubes of micrometer length and about 1.4 nm in diameter. Besides those samples, SWNTs produced by the laser ablation method were also studied, which resulted in similar conclusions. The degree of purification and the content of samples were determined by means of a TEM and an SEM. Some of the samples were exposed to thermal treatment at a moderate pressure, which enhanced their density and provided more reliable contact between the bundles. The initial density of the cloth-like layer produced totaled 2% of the theoretical limit for a bundle consisting of closely packed CNTs 1.4 nm in diameter, while this parameter rose to 70% as a result of the thermal treatment.

Thermal conductance was measured by the comparison method. Small size (roughly $5 \times 2 \times 2$ mm) samples of the cloth-like material were placed parallel to a constantan rod for which the temperature dependence of the thermal conductance was measured previously. Differential thermocouples were affixed directly to the sample and to the constantan rod to measure the temperature drop. One of the ends of the constantan rod was heated, which promoted a heat flow through the rod and the sample onto a cooled contact. The thermal conductance was calculated in a standard manner by processing the data on the temperature drop on the constantan rod and the sample. Due to the proper calibration, the known temperature dependences of the thermal conductivity for various standard materials were well reproduced. The measured temperature dependences of the thermal conductivity for CNT samples of various geometry resulted in similar quantities, which indicates the absence of heat losses at measurements. After measuring the thermal conductance of each of the samples, their electrical resistivity was measured to make a comparison using the four-probe method. The measured temperature dependences of the electroconductivity of the samples assumed a metallic character of conductivity at room temperature and a nonmetallic conductivity at temperatures lower than ~ 150 K. The thermal conductivity κ of some samples measured between 8 and 350 K is shown in Fig. 13. The measurements indicate a smooth increase in κ as the temperature rises from 40 to 350 K. The low temperature part of the dependence $\kappa(T)$ is shown in the inset. At $T \approx 30$ K the slope of the dependence $\kappa(T)$ is changed; below this point the dependence $\kappa(T)$ has a linear shape and is extrapolated to zero at $T = 0$. A similar dependence was observed for all the samples, including those exposed to the thermal treatment. This is followed by the conclusion that the measured thermal conductivity coefficient is related to the bundle samples and does not depend on such effects as heat transfer between the bundles. The observed temperature dependences of the thermal conductivity differ notably from those inherent to graphite, while both the materials contain graphite layers. The thermal conductivity of a high quality crystalline graphite along the graphite plane is governed by acoustic phonons and at $T < 150$ K it is characterized by a temperature dependence $\kappa(T) \sim T^{2-3}$. A further rise in the temperature is accompanied by an increase in the contribution of *umklapp* scattering (phonon–phonon scattering), which causes an abruptly decreasing temperature dependence of

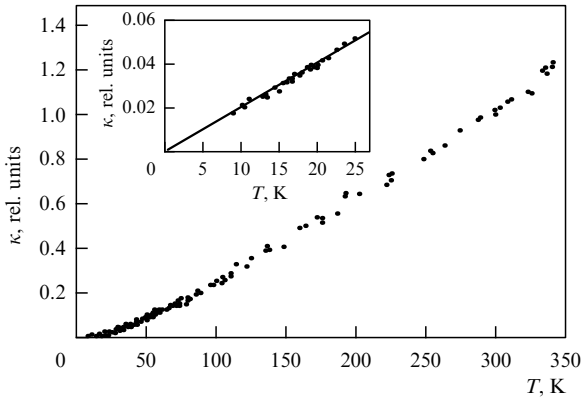

Figure 13. Temperature dependence of the thermal conductivity of a cloth-like sample containing single-walled CNTs. The dependence increases smoothly between 8 and 350 K, changing its slope near 30 K. The low-temperature part of $\kappa(T)$ is shown in the inset. The solid line at $T < 25$ K presents the linear approximation of low temperature data that is extrapolated to zero at a zero temperature [45].

the thermal conductivity. The maximum magnitude of the thermal conductivity of high purity graphite is about 6000 W m^{-1} K^{-1}, while the room temperature value of this parameter is 2000 W m^{-1} K^{-1} [9–11].

The thermal conductivity $\kappa(T)$ of a nanotube bundle sample was calculated on the basis of the measured data taking into account the size of the sample and the degree of its filling with nanotubes. The resulting quantity for a non-treated sample amounted to 35 W m^{-1} K^{-1}, while for a sample undergoing thermal treatment this quantity was as low as 2.3 W m^{-1} K^{-1}. These values are rather incomparable to those for pure metals and graphite.

However, the above quantities were obtained without taking into account the entangled structure of bundles in the samples. As was stated previously, the longitudinal electrocondictivity of an individual bundle exceeds 50–150 times that for a cloth-like layer. It is quite likely that the longitudinal thermal conductivity $\kappa(T)$ of a bundle also considerably exceeds that for a cloth-like layer.

The above estimations show that the thermal conductance of an MWNT is usually higher than that for an SWNT. This is confirmed by numerous measurements. Thus, Ref. [46] reports the results of measurements of the thermal conductance of an individual CNT. Suspended MWNTs not contacting a substrate were studied. The measurements show that the thermal conductance of MWNTs is two orders of magnitude higher than that for the cloth-like material containing SWNTs [45]. Suspended CNTs were formed by means of an electron beam and photolithography on a multilayer silicon nitride/silicon/silicon oxide/silicon structure, which was followed by metallization and etching. The measurement device contained two closely spaced silicon nitride membranes 10×10 μm in size and 0.5 μm in thickness suspended by means of silicon nitride rods 200 μm in length. A thin film Pt resistor fabricated by electron beam lithography was placed on each of the membranes and used as a heater. A nanotube can be placed at a desired point of the measurement device by means of a probe of a scanning probe microscope.

Figure 14 presents the results of measurements of the thermal conductance of an individual MWNT with diameter $d = 14$ nm and 2.5 μm in length [46]. The measurements were performed within the temperature range of 8–370 K. The thermal conductance increases several orders of magnitudes as the temperature rises, reaching at room temperature its maximum value of $\approx 1.6 \times 10^{-7}$ W K^{-1}. This corresponds to a thermal conductivity of ≈ 1200 W m^{-1} K^{-1}. A further increase in the temperature is accompanied by a decrease in the thermal conductivity.

The ballistic character of heat transport was observed by the authors of Ref. [43], who studied SWNTs produced by the electrical arc method. The material synthesized consisted of bundles about 100 μm in diameter and up to 2 mm in length containing nanotubes ~ 500 nm in length and ~ 2 nm in diameter. However, more thin bundles were also observed, on whose ends individual nanotubes were visible.

The results of direct measurements of electrical conductance and thermal conductance are shown in Fig. 15. As is seen, the measured magnitudes hardly depend on the length of the CNT up to $L \approx 8.5$ μm. One can believe that ballistic behavior occurs for shorter nanotubes. This conclusion is confirmed by the measured absolute magnitudes of the electrical conductance and thermal conductance, which are in good agreement with the above relations (1) and (4). Thus,

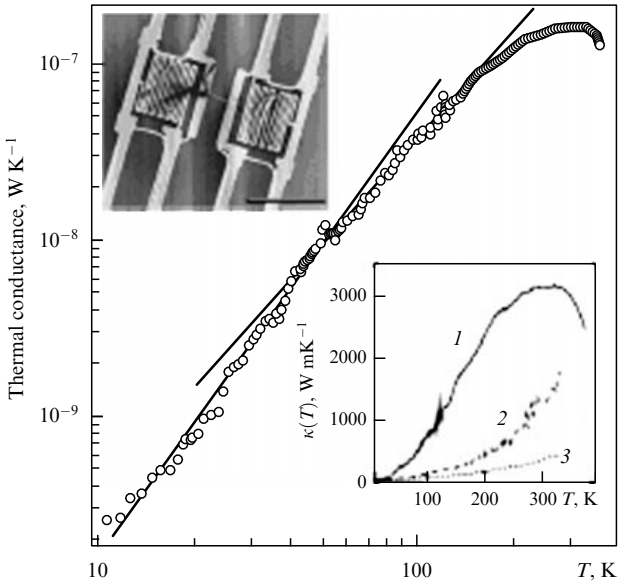

Figure 14. Thermal conductance of an individual MWNT 14 nm in diameter [23]. Solid lines present the linear approximation (logarithmic coordinates) of data in various temperature ranges. The slopes of these lines are 2.50 and 2.01, respectively. The bottom inset: curve *1* presents the dependence $\kappa(T)$ for an individual MWNT with $d = 14$ nm in diameter; curves *2* and *3* correspond to large ($d = 200$ nm) and small ($d = 80$ nm) MWNT bundles. The upper inset shows an SEM image of the suspended sample containing an individual MWNT. The scale bar is 10 μm.

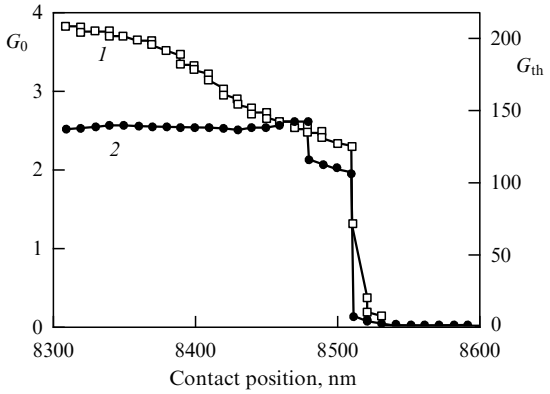

Figure 15. The thermal conductance (*1*) and electric conductance (*2*) of an individual CNT placed on a crystalline graphite substrate measured at room temperature in vacuum conditions [43].

assuming that the heat transport is due to the ballistic mechanism, one obtains on the basis of Eqns (4) and (5) the magnitude $G_{th} = 120G_0$ for a nanotube (10, 10), which is very close to the measured quantity $G_{th} \approx 128G_0$. The measured value of electrical conductance is about twice as much as the quantum ballistic magnitude $G_0 = 2e^2/h = 12.9$ kΩ^{-1}.

The above conclusions on the ballistic heat transport in SWNTs contradict the results of measurements of temperature dependences of the thermal conductance of an individual suspended SWNT within the temperature range of 300–800 K [47]. According to Eqns (4) and (5), in the case of prevalence of the ballistic mechanism of heat transport, the thermal conductance of a CNT is proportional to the temperature. However, the measurements [47] show an inversely proportional temperature dependence of this para-

meter. Therefore, one can conclude that the mechanism of heat transport in CNTs is more complicated. The temperature dependences of the thermal conductance were determined in Ref. [47] on the basis of the solution of the heat conductivity equation for a nanotube using the measured current–voltage characteristics. The temperature of the nanotubes ranged between 250 and 400 K.

Suspended SWNTs were grown between Pt contacts over grooves etched by lithography. The geometry of the nanotubes was determined by means of an SEM and AFM. The electrical measurements were performed in vacuum conditions (roughly 10^{-6} Torr) within the temperature range between 250 and 400 K. Vacuum conditions provided the thermal isolation of CNTs so that practically all the joule heat released in the nanotube was removed to the substrate due to thermal conductivity. Estimations imply that the contribution of thermal radiation to the heat balance of a nanotube does not exceed fractions of a percent. The temperature dependence of the thermal conductance of a single-walled CNT ≈ 2.6 μm in length and ~ 1.7 nm in diameter was evaluated as a result of the treatment of the current–voltage characteristic.

The temperature dependence of the thermal conductivity was determined through the solution of the reverse task so that the dependence $\kappa(T)$ providing the measured data at specified magnitudes of the applied voltage and power supply was found. The bias voltage was chosen to be quite high ($V > 0.3$ V) to ensure a notable self-heating of the nanotube. The charge transport in this range of the bias voltage is due to the scattering of electrons on optical phonons, which determines the dependence of the resistance on the electron mean free path l_{op} relating to this type of scattering, $R \sim (h/4e^2)(L/l_{op})$. Since the electron mean free path l_{op} is inversely proportional to the concentration of optical phonons N_{op}, which in turn is proportional to the temperature within the temperature range under consideration, this results in the linear temperature dependence of the resistivity $R \sim 1/l_{op} \sim N_{op} \sim T$. The value of the temperature is determined by the heat balance between the joule heating and the thermal conductivity. The above approach to determining the temperature dependence of the thermal conductivity of a CNT allows minimization of the influence of contact resistance or contact thermal conductance on the measured results.

Figure 16 presents the temperature dependence of the thermal conductivity of a CNT [47]. At first glance this dependence corresponds to the phonon–phonon *umklapp* scattering determining the dependence $\kappa \sim 1/T$. However, at elevated temperatures one can also see a weak effect resulting in a sharper temperature dependence. The authors of Ref. [47] ascribe this effect to three-phonon scattering processes whose rate is proportional to T^2. Taking into account such effects results in the temperature dependence of thermal conductivity coefficient $\kappa \sim 1/(\alpha T + \beta T^2)$, where α and β are constants. In the case of an SWNT, such processes most likely include three-phonon anharmonic interaction of two acoustic and one optical phonon, which is caused by the rise in the concentration of optical phonons as the temperature and the bias voltage increase. The thermal conductivity peaks at room temperature, which is related to an increase in the contribution of the diffusion mechanism of the thermal conduction that is characterized by a decreasing temperature dependence of the thermal conductivity. The magnitude of the specific thermal conductivity coefficient measured in the experiments

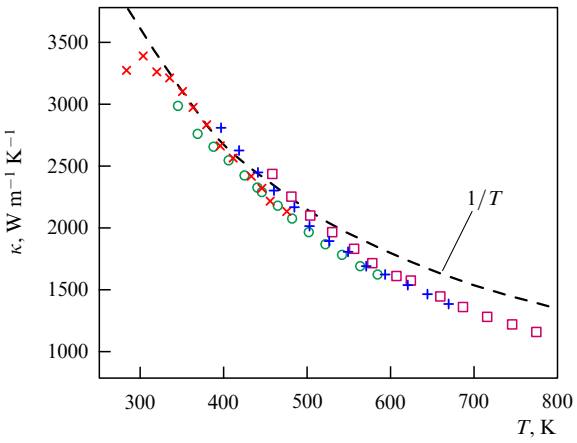

Figure 16. Dependence of the thermal conductivity coefficient on the mean temperature evaluated as a result of processing the current–voltage characteristic at high bias voltages [47]. Various symbols relate to different magnitudes of the ambient temperature. The broken line shows the dependence $\kappa \sim 1/T$ corresponding to the umklapp phonon–phonon scattering. Note the contribution of three-phonon interaction involving one optical and two acoustical phonons, which is proportional to $1/T^2$ and manifests itself at elevated temperatures.

under consideration amounts to about $G \sim 2.4$ nW K^{-1}, which is about an order of magnitude lower than the estimation performed on the basis of Eqns (4) and (5) assuming the ballistic mechanism of heat transport. For a nanotube ≈ 2.6 μm in length and ~ 1.7 nm in diameter, this corresponds to the room temperature thermal conductivity coefficient $\kappa \sim 3500$ W m^{-1} K^{-1}. At $T = 800$ K this parameter decreases to the level of 1000 W m^{-1} K^{-1}.

One should note that when measuring the thermal conductivity by the above-described method the main difficulty relates to the necessity of quantitative evaluation of the temperature of the nanotube. The authors of Ref. [47] have managed to overcome this difficulty using the known fact that an SWNT is destroyed in the presence of oxygen at a temperature of 800–900 K. This permits verification of the procedure of evaluation of the nanotube's temperature by the solution of the heat conductivity equation matching the condition of breakdown of the nanotube. This approach has provided a room temperature thermal conductivity within the range of 2800–3900 W m^{-1} K^{-1} and in a narrower range of 1000–1160 W m^{-1} K^{-1} for $T = 800$ K.

The temperature dependences of the thermal conductivity of SWNTs measured at low [48] and enhanced [47] temperatures are compared in Fig. 17. As is seen, the room temperature thermal conductivity value measured by various authors differ by 20%. Such a difference can be explained by a difference in the length of the nanotubes under investigation ($L \sim 2.8$ μm in [48] and 2.6 μm in [47]), as well as by a difference in the quality of contacts.

As was noted above (see Section 2.1), one of the important issues arising in the analysis of measured transport characteristics of CNTs relates to the necessity of properly taking into account the role of contacts. In this connection, a recently-developed noncontact method of heating a sample and measuring the temperature distribution along the nanotube [73] is of interest. This method is based on the measurement of the Raman spectrum, which is sensitive to the temperature. Such an approach allows estimating the thermal conductivity coefficient and the contribution of contacts to the heat

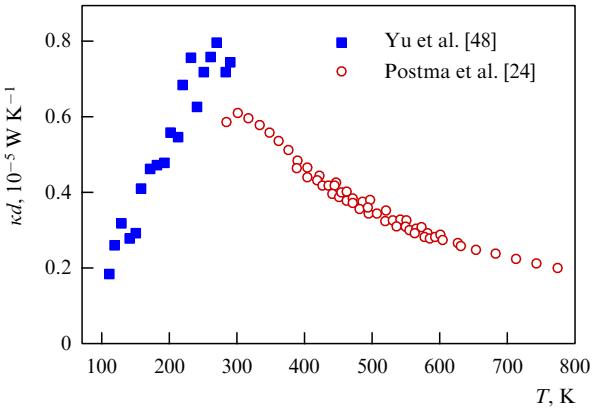

Figure 17. Comparison of temperature dependences of the thermal conductance of an individual SWNT (corrected for the nanotube's diameter $\kappa d = GL/\pi b$) measured at elevated [24] and low temperatures [48].

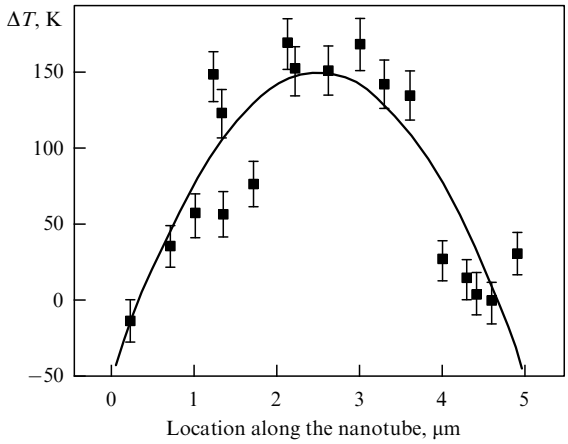

Figure 18. Distribution of the temperature along a single-walled nanotube measured by the use of the Raman scattering method. The nanotube is suspended over a groove 4.7 μm in width and heated by laser irradiation at a power of about 100 μW [73].

balance for a single-walled nanotube. A single-walled CNT 1.66 nm in diameter and over 5 μm in length was grown by the CVD method directly under a groove 5 μm in width etched in a Si/SiO_2 substrate. The nanotube was locally heated by solid state laser radiation with $\lambda = 532$ nm focused on a spot 0.36 μm in diameter by means of a special optical system. The temperature of the irradiated region of the CNT was evaluated on the basis of a measurement of the temperature shift of the G-band in the Raman spectrum obtained with the use of the second harmonic of an Nd:glass laser (wavelength 532 nm) with power between 93 μW and 1.4 mW. The measurements indicated a typical drop in the temperature along the nanotube of about 150 K. This method of measurement does not allow determination of the thermal conductivity coefficient for a CNT, because the magnitude of laser power absorbed by the nanotube is unknown. However, this approach offers an opportunity to determine the ratio of contributions from the nanotube and the contacts to the heat balance. The results of measurements of this ratio for various samples of SWNTs range within a rather wide region — between 0.02 and 17, which indicates the high sensitivity of the transport characteristics of CNTs to the synthesis conditions.

Figure 18 presents a temperature profile along the axis of a single-walled nanotube suspended over a groove 4.7 μm in width as measured by Raman scattering [73]. The measurements indicate the negligible role of the ballistic mechanism of heat transport in the nanotubes under investigation. This follows from a considerable temperature gradient along the nanotube, which is possible only if there is a prevalence of the diffusion mechanism of heat transport. This conclusion assumes that the mean free path of an acoustic phonon related to scattering on structural defects is much shorter than the longitudinal size of the nanotube (5 μm). One can expect that the further development of contactless methods of heating CNTs and measuring the longitudinal temperature distribution will result in obtaining reliable data on temperature dependences of the thermal conductivity of CNTs not exposed to the influence of contacts.

In conclusion, one can note that the measured absolute magnitudes of the thermal conductivity coefficient are of the same order or slightly lower than those calculated by Eqn (4) and (5), assuming the ballistic mechanism of heat transport. However, a decreasing temperature dependence of this parameter observed at an elevated temperature is in contradiction with this conclusion. Therefore, one can believe that ballistic heat transport prevails only within a low temperature range, while at elevated temperatures (above room temperature) intensive formation of defects occurs; so the scattering on these defects suppresses the ballistic character of phonon propagation and causes a corresponding decrease in the thermal conductivity coefficient.

4. Conclusion

Tables 3 and 4 below contain experimental data on the transport characteristics of CNTs. In addition, relevant data on carbon filaments, crystalline graphite, and diamond are also given for comparison. As is seen, the measured magnitudes of the electrical resistance of CNTs are characterized by a spread from tens of ohms up to several megaohms. Such a considerable spread indicates, on the one hand, the absence of a reliable contact in many measurements and, on the other hand, the occurrence of an essential dependence of the parameters of CNTs on the methods of their synthesis and specific conditions at which the particular sample has been synthesized. Therefore, one can conclude that since nanotubes with predefined characteristics can not yet be synthesized, it is premature to consider the possibility of using them as elements of nanoelectronic devices. The solution to this technological problem presents a serious challenge for researchers who are already concentrating their efforts on the development of methods of separation and enrichment of CNTs over their geometry parameters and electronic characteristics [70 – 72].

The author cordially thanks L A Chernozatonskii for the helpful criticism.

References

1. Eletskii A V *Usp. Fiz. Nauk* **172** 401 (2002) [*Phys. Usp.* **45** 369 (2002)]
2. Shakir M I et al. *Nanotechnology* **17** R41 (2006)
3. De Jonge A N, Bonard J N *Proc. R. Soc. London A* **362** 2239 (2004)
4. Cheng Y, Zhou O *C.R. Phys.* **4** 1021 (2003)
5. Futaba D N et al. *Nature Mater.* **5** 987 (2006)
6. Kamat P V *Nanotoday* **1** (4) 20 (2006)
7. Jang J E et al. *Appl. Phys. Lett.* **87** 163114 (2005)

Table 3. The magnitudes of the resistance (resistivity) of CNTs measured by different authors. The third column of the table contains the parameters determining the temperature dependence of the electrical resistance. If this parameter is the forbidden band gap or the activation energy ΔE, the resistance $R \sim \exp(\Delta E/T)$, in the case of power-like temperature dependence the power index α is given.

Material	Resistance, kΩ (room temperature)	Forbidden gap width or the activation energy, eV, or the power index of the dependence $R(T)$	References
CNT bundle produced by the electrical arc method	6.5×10^3		[49]
Film of aligned CNTs	2×10^4		[50]
Individual MWNT	$(0.82-12) \times 10^3$		[51]
Individual MWNT	$(5.1-5.8) \times 10^6$		[52]
Individual MWNT	$(0.3-3) \times 10^5$	0.17 – 0.26	[53]
Composite CNT – epoxy	3.4×10^4		[54]
MWNT		0.08	[55]
MWNT	$(0.53-1.9) \times 10^3$	0.19 – 0.29	[56]
Boron-doped MWNT	$(0.7-7.7) \times 10^2$	0.055 – 0.070	[56]
MWNTs produced by the CVD method	3.5 ± 2.6		[35]
MWNTs produced by the electrical arc method	10 – 20		[36]
MWNTs 3 μm in length and 30 – 100 nm in diameter produced by the CVD method	47 (averaged)		[57]
MWNT bundles 0.66 – 2.82 μm in diameter	$30-8.8 \times 10^3$		[58]
SWNT bundle produced by the laser ablation method	14		[23]
SWNT bundle	1.5		[59]
Individual SWNTs 95 – 590 nm in length	1.5 – 37		[22]
SWNT stripes 2 × 6 mm in size	5×10^3		[60]
Individual SWNT	~ 10	$R \sim T^{\alpha}$, $\alpha \approx -1.4$	[24]
MWNT 4 μm in length	60		[62]
Individual metallic SWNT	2.5×10^3	$R \sim T^{\alpha}$, $\alpha \approx -0.6$	[25]
Individual semiconductive SWNT	10^4	$R \sim T^{\alpha}$, $\alpha \approx -3.4$	[25]
Individual MWNT 3 – 11 μm in length and 30 – 60 nm in diameter	130		[63]
Individual MWNT 1.2 μm in length and 3 nm in diameter	20		[64]
Individual MWNT 100 and 50 nm in outer and inner diameters	34.4 Ω		[38]
Individual MWNT 2.6 μm in length and 8.6 nm in diameter	2.4 ($T = 520$ K)		[74]
Individual MWNT 2.5 μm in length and 15.1 nm in diameter	1.7 ($T = 520$ K)		[74]
Cloth-like SWNT layer 3 × 0.2 mm in size	0.012		[75]
Cloth-like SWNT layer 2 × 0.2 × 25 mm in size	0.0032	$R \sim T^{\alpha}$, $\alpha \approx -0.55$	[76]
Carbon fiber ~ 150 nm in diameter	4.4×10^3		[65]
Diamond	$\sim 10^{26}$	5.47	[9]
Graphite (along the hexagonal plane)	50	0.04	[9]
	Resistivity, kΩ μm^{-1} (room temperature)		
MWNT 9 nm in diameter	10		[61]
Individual MWNT 4 – 10 μm in length and 83 – 225 nm in diameter	0.69		[37]
CVD-grown individual SWNT	10 ± 2		[26]
SWNT 4 mm in length	6 – 7		[31]

Table 4. The thermal conductivity coefficient of CNTs measured by various authors. Parameter α presents the index of the power-like temperature dependence of the thermal conductivity $\kappa(T) \sim T^{\alpha}$.

Material	Temperature, K	Thermal conductivity, W m^1 K^{-1} (thermal conductance of a sample, W K^{-1}) room temperature	α	References
Cloth-like SWNT layer $5 \times 2 \times 2$ mm in size	8 – 350	35	~ 1	[45]
MWNT 14 nm in diameter and 2.5 μm in length	8 – 370	3000 (1.6×10^{-7})		[46]
Cloth-like MWNT layer		20		[66]
SWNT bundle		250		[67]
MWNT $\sim$ 2 nm in diameter and 500 nm in length		(3.6×10^{-8})		[43]
MWNT 10 nm in diameter	600	600		[68]
SWNT 1.7 nm in diameter and 2.6 μm in length	300 – 800	3500	-1	[47]
SWNT film 35 nm in thickness (nontreated)	50 – 300	30	1.3	[69]
SWNT film 100 nm in thickness (purified)	10 – 300	90	1.1	[69]

8. Lucci M et al. *Sensors Actuators B* **111 – 112** 181 (2005)
9. Dresselhaus M S, Dresselhaus G, Eklund P C *Science of Fullerenes and Carbon Nanotubes* (San Diego: Academic Press, 1996)
10. Saito R, Dresselhaus M S, Dresselhaus G *Physical Properties of Carbon Nanotubes* (London: Imperial Colledge Press, 1998)
11. Dresselhaus M S, Dresselhaus G, Avouris P (Eds) *Carbon Nanotubes*: *Synthesis, Structure, Properties, and Applications* (Berlin: Springer, 2001)
12. Fischer J E, in *Carbon Nanomaterials* (Ed. Y Gogotsi) (Boca Raton, Fl.: CRC/Taylor & Francis, 2006) p. 41
13. Eletskii A V *Usp. Fiz. Nauk* **174** 1191 (2004) [*Phys. Usp.* **47** 1119 (2004)]
14. Eletskii A V *Usp. Fiz. Nauk* **177** 233 (2007) [*Phys. Usp.* **50** 225 (2007)]
15. Loiseau A et al. (Eds) *Understanding Carbon Nanotubes*: *From Basics to Applications* (Berlin: Springer, 2006)
16. Rotkin S V, Subramoney S (Eds) *Applied Physics of Carbon Nanotubes*: *Fundamentals of Theory, Optics and Transport Devices* (Berlin: Springer, 2005)
17. Ebbesen T W (Ed.) *Carbon Nanotubes*: *Preparation and Properties* (Boca Raton, Fl.: CRC Press, 1997)
18. Huang N Y et al. *Phys. Rev. Lett.* **93** 075501 (2004)
19. Bocharov G S, Eletskii A V *Zh. Tekh. Fiz.* **77** (4) 107 (2007) [*Tech. Phys.* **52** 498 (2007)]
20. Bonard J-M et al. *Phys. Rev. B* **67** 115406 (2003)
21. Vorob'eva A I *Usp. Fiz. Nauk* **179** 243 (2009) [*Phys. Usp.* **52** 225 (2009)]
22. Gao B et al. *Phys. Rev. Lett.* **95** 196802 (2005)
23. Kane C L et al. *Europhys. Lett.* **41** 683 (1998)
24. Postma H W Ch et al. *Phys. Rev. B* **62** R10653 (2000)
25. Skákalová V et al. *Phys. Rev. B* **74** 085403 (2006)
26. Sundqvist P et al. *Nano Lett.* **7** 2568 (2007)
27. Park J-Y et al. *Nano Lett.* **4** 517 (2004)
28. Gómez-Navarro C et al. *Nature Mater.* **4** 534 (2005)
29. Biel B et al. *Phys. Rev. Lett.* **95** 266801 (2005)
30. Javey A et al. *Phys. Rev. Lett.* **92** 106804 (2004)
31. Li S et al. *Nano Lett.* **4** 2003 (2004)
32. Dürkop T et al. *Nano Lett.* **4** 35 (2004)
33. Li S et al. *Nano Lett.* **4** 753 (2004)
34. Javey A et al. *Nature* **424** 654 (2003)
35. Lan C et al. *Appl. Phys. Lett.* **91** 093105 (2007)
36. Graugnard E et al. *Phys. Rev. B* **64** 125407 (2001)
37. Lan C, Zakharov D N, Reifenberger R G *Appl. Phys. Lett.* **92** 213112 (2008); Lan C et al. *Nanotechnology* **19** 125703 (2008)
38. Li H J et al. *Phys. Rev. Lett.* **95** 086601 (2005)
39. Collins P G et al. *Phys. Rev. Lett.* **86** 3128 (2001)
40. Frank S et al. *Science* **280** 1744 (1998)
41. Berger C et al. *Appl. Phys. A* **74** 363 (2002)
42. Yamamoto T, Watanabe S, Watanabe K *Phys. Rev. Lett.* **92** 075502 (2004)
43. Brown E et al. *Appl. Phys. Lett.* **87** 023107 (2005); *AIP Conf. Proc.* **723** 91 (2004)
44. Chang C W et al. *Phys. Rev. Lett.* **101** 075903 (2008)
45. Hone J, Whitney M, Zettl A *Synthetic Met.* **103** 2498 (1999); Hone J et al. *Phys. Rev. B* **59** R2514 (1999)
46. Kim P et al. *Phys. Rev. Lett.* **87** 215502 (2001)
47. Pop E et al. *Nano Lett.* **6** 96 (2006)
48. Yu C et al. *Nano Lett.* **5** 1842 (2005)
49. Song S N et al. *Phys. Rev. Lett.* **72** 697 (1994)
50. de Heer W A et al. *Science* **268** 845 (1995)
51. Dai H, Wong E W, Lieber C M *Science* **272** 523 (1996)
52. Ebbesen T W et al. *Nature* **382** 54 (1996)
53. Kasumov A Yu et al. *Europhys. Lett.* **43** 89 (1998)
54. Wang Q H et al. *Appl. Phys. Lett.* **70** 3308 (1997)
55. Carroll D L et al. *Phys. Rev. Lett.* **81** 2332 (1998)
56. Wei B et al. *Appl. Phys. Lett.* **74** 3149 (1999)
57. Dohn S, Mølhave K, Bøggild P *Sensor Lett.* **3** 300 (2005)
58. Wakaya F, Katayama K, Gamo K *Microelectron. Eng.* **67 – 68** 853 (2003)
59. Appenzeller J et al. *Appl. Phys. Lett.* **78** 3313 (2001)
60. Bozhko A D et al. *Appl. Phys. A* **67** 75 (1998)
61. Bachtold A et al. *Nature* **397** 673 (1999); *Phys. Rev. Lett.* **84** 6082 (2000)
62. de Pablo P J et al. *Appl. Phys. Lett.* **75** 3941 (1999)
63. Bussolotti F et al. *Phys. Rev. B* **76** 125415 (2007)
64. Yaish Y et al. *Phys. Rev. Lett.* **92** 046401 (2004)
65. Zhang L et al. *Appl. Phys. Lett.* **84** 3972 (2004)
66. Yi W et al. *Phys. Rev. B* **59** R9015 (1999)
67. Hone J et al. *Appl. Phys. Lett.* **77** 666 (2000)
68. Chiu H-Y et al. *Phys. Rev. Lett.* **95** 226101 (2005)
69. Itkis M E et al. *Nano Lett.* **7** 900 (2007)
70. Samsonidze G G et al. *Appl. Phys. Lett.* **85** 1006 (2004)
71. Arnold M S et al. *Nature Nanotechnol.* **1** 60 (2006)
72. Hersam M C *Nature Nanotechnol.* **3** 387 (2008)
73. Hsu I-K et al. *Appl. Phys. Lett.* **92** 063119 (2008)
74. Wei B Q et al. *Appl. Phys. Lett.* **79** 1172 (2001)
75. Gaál R, Salvetat J-P, Forró L *Phys. Rev. B* **61** 7320 (2000)
76. Zahab A et al. *Phys. Rev. B* **62** 10000 (2000)